OPEN ACCESS

The spinning ball spiral

New Journal of Physics
The open-access journal for physics

The spinning ball spiral

Guillaume Dupeux, Anne Le Goff, David Quéré and Christophe Clanet[1]
PMMH, UMR7636 du CNRS, ESPCI, 10 rue Vauquelin, 75005 Paris, France
and
LadHyX, UMR7646 du CNRS, Ecole Polytechnique, 91128 Palaiseau, France
E-mail: clanet@ladhyx.polytechnique.fr

New Journal of Physics **12** (2010) 093004 (12pp)
Received 3 March 2010
Published 2 September 2010
Online at http://www.njp.org/
doi:10.1088/1367-2630/12/9/093004

Abstract. We discuss the trajectory of a fast revolving solid ball moving in a fluid of comparable density. As the ball slows down owing to drag, its trajectory follows an exponential spiral as long as the rotation speed remains constant: at the characteristic distance $\mathcal{L}$ where the ball speed is significantly affected by the drag, the bending of the trajectory increases, surprisingly. Later, the rotation speed decreases, which makes the ball follow a second kind of spiral, also described in the paper. Finally, the use of these highly curved trajectories is shown to be relevant to sports.

Contents

[1] Author to whom any correspondence should be addressed.

1. Introduction

Since Galileo, spheres have been used by physicists to probe movement and friction [13, 14, 27]. In the context of hydrodynamics, in particular, the motion of a solid sphere (radius R, velocity U_0, density ρ_s) in a quiescent liquid (viscosity η, density ρ) is the paradigm for characterizing the laws of friction at low and high Reynolds numbers.

For low Reynolds number ($Re = \rho U_0 R/\eta \ll 1$), Stokes [30] established that the drag force experienced by the solid during its motion is $F = 6\pi\eta U_0 R$. This very classical result was then verified by several authors in the range $Re < 1$ [8, 24]. For high Reynolds numbers, Newton [22] was probably the first to propose an heuristic expression for the drag: $F = 1/2 C_D \rho U_0^2 \pi R^2$, where C_D is a coefficient provided by the experiments. According to Eiffel [12], C_D is of the order of 0.4, a value later confirmed in the range $10^3 < Re < 2 \times 10^5$ [28]. For intermediate Reynolds numbers ($1 < Re < 10^3$), the asymptotic expansion method proposed by Oseen [23] led to lots of theoretical developments [4]. Beyond $Re \approx 2 \times 10^5$, the resistance crisis experienced by the sphere once the boundary layer becomes turbulent has also been studied in depth [1, 17, 29].

For spinning spheres, according to Barkla and Auchterloniet [2], the work seems to go back to Robins [25] and then Magnus [18], who got the credit for the associated lift force. Besides these academic studies, the widespread use of balls in sports also motivated many studies, in baseball [21] and golf [9] in particular, a review of which can be found in [20]. Most of these studies consider a lift force $F_L = 1/2 C_L \rho U_0^2 \pi R^2$, where the lift coefficient C_L is known to increase with the spin parameter $S = R\omega_0/U_0$.

Here, we study the trajectory of spinning spheres in water and try to understand their surprisingly curved trajectory, an example of which is presented in figures 1 and 2. In figure 1, the trajectory is decomposed into eight images, whereas in figure 2, the same sequence is presented within a single image by superimposing the successive positions of the ball. Both figures reveal a spiral trajectory. With solid friction and rotation, similar curved trajectories can be obtained, for example in French billard [6] and in lawn bowls [7]. In figure 2, we also observe the formation of an air cavity behind the sphere, a consequence of the high speed of penetration [5, 10, 11, 15, 16, 19, 32]. The bending of the trajectory starts as soon as the ball enters the bath, as reported in [31] for vertical impacts. Our aim here is to focus on the spiral trajectory and to discuss its relevance to sports.

2. Experimental facts

The projectiles used in this study are balls made of either polypropylene ($\rho_s \simeq 920\,\mathrm{kg\,m^{-3}}$) or polyacetal ($\rho_s \simeq 1400\,\mathrm{kg\,m^{-3}}$), a few millimetres in size. Spin and high velocities (20–50 $\mathrm{m\,s^{-1}}$) are achieved using a slingshot, consisting of a forked stick attached to a pocket by two rubber strips. The velocity can be varied by tuning the average tension applied to the rubbers, whereas the spin is controlled by the difference in tension between them: the motion is a pure translation when the extension of the two arms is symmetric, and spinning occurs when one strip is more stretched than the other. Both translational and spin velocities at the moment of impact U_0 and ω_0 are measured on the images recorded with a high speed video camera. Rotation is made visible by drawing a line on the equator and illuminating the spheres.

The effect of spin is illustrated in figure 3. Without rotation ($\omega_0 = 0$), the ball goes straight (figure 3(a)). With a bottom spin ($\omega_0 > 0$), figure 3(b) shows that the ball deviates upwards;

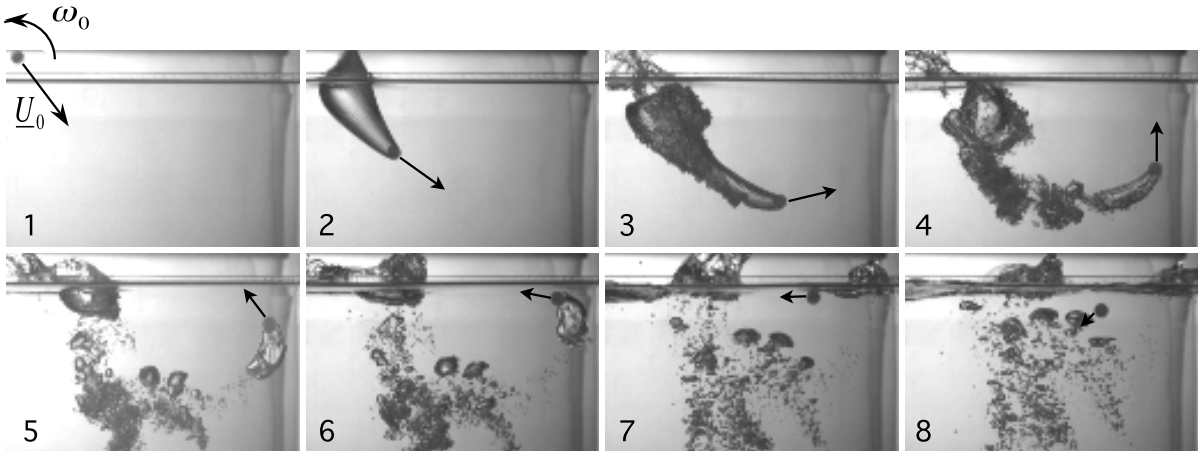

Figure 1. Chronophotography of the impact of an iso-density sphere ($R = 3.5$ mm) penetrating a bath of water at $U_0 = 35\,\mathrm{m\,s^{-1}}$ and spinning at $\omega_0 \approx 1200\,\mathrm{rad\,s^{-1}}$. The time step between images is not constant. $t = 0$ is the impact time, $t_1 = -0.5$ ms, $t_2 = 2.8$ ms, $t_3 = 13$ ms, $t_4 = 42$ ms, $t_5 = 76$ ms, $t_6 = 101$ ms, $t_7 = 169$ ms and $t_8 = 216$ ms. The arrows indicate the sphere velocity.

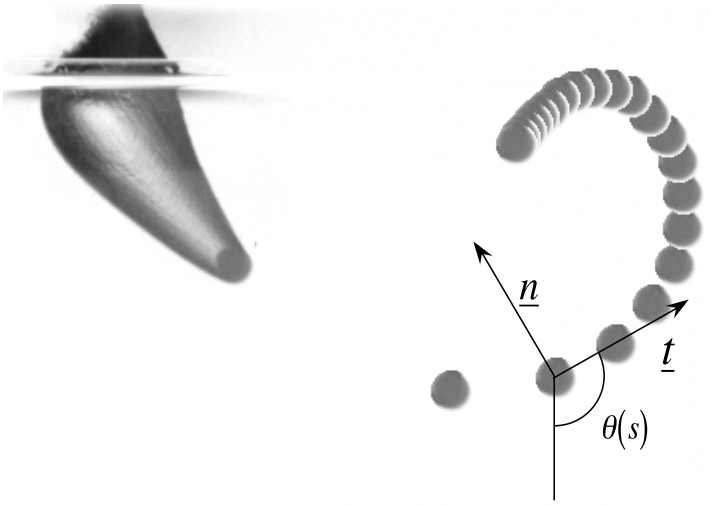

Figure 2. Multi-pose image showing the trajectory of the ball of figure 1. The time step between successive ball locations is $\Delta t = 10$ ms. This image reveals a spiral trajectory.

it is even able to escape from the bath (last two images). Finally, for top spin ($\omega_0 < 0$), the ball deviates downwards (figure 3(c)). We focus now on the bottom spin case and show in figure 4(a) the trajectory of a polypropylene ball ($\rho_s/\rho = 0.92$) of radius $R = 3.5$ mm thrown in a water bath at a velocity $U_0 = 27\,\mathrm{m\,s^{-1}}$, with a spin rate $\omega_0 = 1000\,\mathrm{rad\,s^{-1}}$ and an impact angle $\theta_0 = 70^\circ$ (defined from the vertical). In this trajectory, the constant time step between two data is $\Delta t = 384\,\mu$s. Clearly, the velocity of the ball decreases as it moves through water (figure 4(a)). The evolution of the ball velocity is reported in figure 4(b) as a function of the curvilinear location s ($s = 0$ at impact). The semi-log presentation stresses that the velocity decreases exponentially with s. The characteristic length of the decrease is here 5.5 cm. Despite

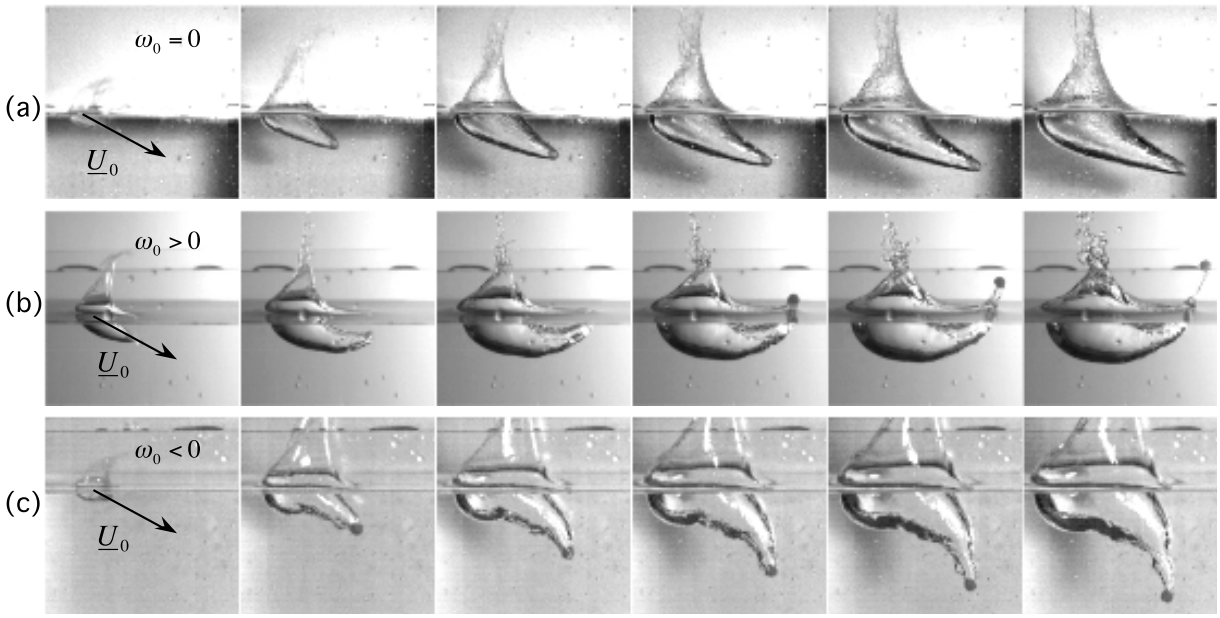

Figure 3. Effect of spin on the trajectory of a sphere (density ρ_s) after impact in water: (a) $U_0 = 33\,\mathrm{m\,s^{-1}}$, $R = 3.5\,\mathrm{mm}$, $\rho_s = 1410\,\mathrm{kg\,m^{-3}}$, $\omega_0 = 0\,\mathrm{rad\,s^{-1}}$, time step between images $\Delta t = 2\,\mathrm{ms}$. (b) $U_0 = 20\,\mathrm{m\,s^{-1}}$, $R = 2.4\,\mathrm{mm}$, $\rho_s = 920\,\mathrm{kg\,m^{-3}}$, $\omega_0 = 1740\,\mathrm{rad\,s^{-1}}$, $\Delta t = 3.75\,\mathrm{ms}$. (c) $U_0 = 24\,\mathrm{m\,s^{-1}}$, $R = 2.4\,\mathrm{mm}$, $\rho_s = 920\,\mathrm{kg\,m^{-3}}$, $\omega_0 = -1740\,\mathrm{rad\,s^{-1}}$, $\Delta t = 3.2\,\mathrm{ms}$. The trajectory bends only if spin is present and the sign of its curvature changes with the sign of the spin.

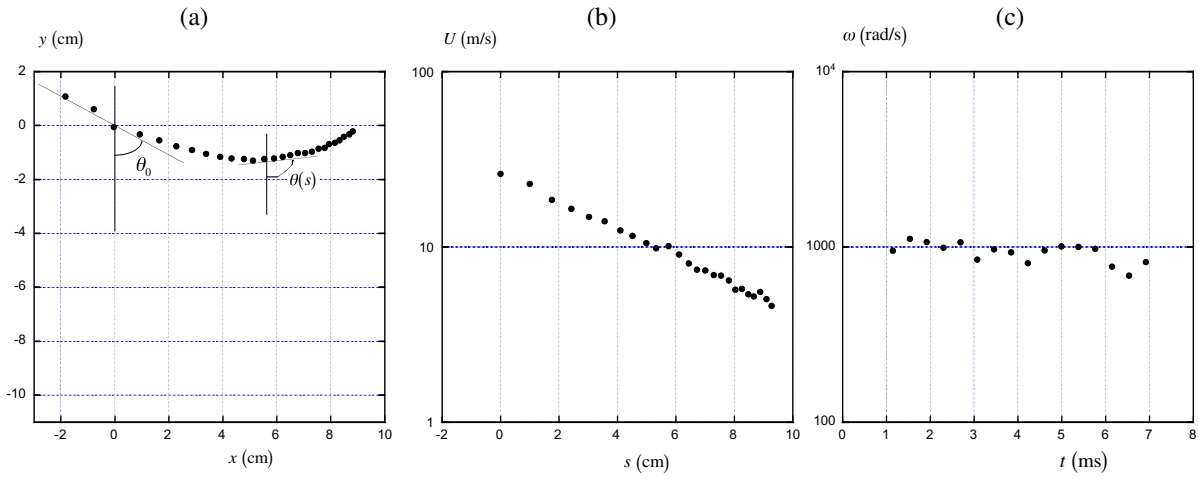

Figure 4. (a) Trajectory of a ball (radius $R = 3.5\,\mathrm{mm}$, density $\rho_s = 920\,\mathrm{kg\,m^{-3}}$) impacting water with a velocity $U_0 = 27\,\mathrm{m\,s^{-1}}$, a spin $\omega_0 = 1000\,\mathrm{rad\,s^{-1}}$ and an inclination angle $\theta_0 = 70^\circ$. The time step between two data points is $\Delta t = 384\,\mu\mathrm{s}$. (b) Evolution of the corresponding velocity as a function of the curvilinear location s in a semi-log plot. (c) Time variation of the corresponding rotation speed ω of the ball.

a strong variation in the velocity, the spin rate ω remains almost constant as the ball moves through water, as demonstrated in figure 4(c). This difference is discussed in the following section and is shown to be the key fact to account for the spiral trajectory.

3. Model

3.1. Drag

The motion of the sphere of mass M is described in the Serret–Frenet coordinate system $(\underline{t}, \underline{n})$ introduced in figure 2. We first focus on the direction $\underline{t}$. The Reynolds number $Re = \rho U_0 R/\eta$ is of the order of 10^4, which implies a drag $F \approx 1/2\rho U^2 \pi R^2 \cdot C_\mathrm{D}$, with $C_\mathrm{D} \approx 0.4$ [28]. The equation of motion along $\underline{t}$ thus is written as

$$M\left(1 + C_\mathrm{M}\frac{\rho}{\rho_s}\right) U\frac{\mathrm{d}U}{\mathrm{d}s} = -\frac{1}{2}\rho U^2 \pi R^2 \cdot C_\mathrm{D}. \tag{1}$$

In this equation, C_M stands for the added mass coefficient, which, for a sphere, is of the order of $1/2$, independent of the speed U [3]. Using the condition $U(s=0) = U_0$, equation (1) can be integrated as

$$U(s) = U_0\,\mathrm{e}^{-s/\mathcal{L}} \tag{2}$$

with

$$\mathcal{L} = \frac{8}{3}\frac{\bar{\rho}}{C_\mathrm{D}} R \quad \text{with } \bar{\rho} = \left(1 + C_\mathrm{M}\frac{\rho}{\rho_s}\right)\frac{\rho_s}{\rho}. \tag{3}$$

The velocity thus decreases exponentially in water, with a characteristic penetration length $\mathcal{L} \approx 7\bar{\rho}R \approx 10R$. This behaviour agrees with the results displayed in figure 4(b). We deduce from such measurements the value of $\mathcal{L}$ for different systems. Our data are presented in figure 5 as a function of the length $\bar{\rho}R$ and compared to the results obtained by May [19] and Truscott and Techet [31]. All the data collapse in the same curve, $\mathcal{L} \approx 7\bar{\rho}R$, in good agreement with equation (3). This comparison underlines that the entrained air cavity visible in figures 1–3 does not significantly affect the drag on the sphere. The time variation of the velocity can finally be deduced from equation (1), which classically yields $U(t) = U_0/(1 + t/\tau)$, where $\tau = \mathcal{L}/U_0$ is the characteristic slowing time of the ball.

In equation (1) and in the above discussion, we neglected the effect of gravity. This assumption remains valid as long as the drag F is large compared to the Archimedean force $4\pi/3(\rho_s - \rho)gR^3$. Using the expression for the drag, we conclude that the low gravity regime is achieved as long as $U \gg U*$, where $U^{*2} = 8/3C_\mathrm{D}|\rho_s/\rho - 1|gR$. This condition is always fulfilled in the iso-density case but it fails otherwise at the 'end' of the trajectory, when the velocity of the ball vanishes. In this paper, we focus on the hydrodynamic effects and do not address the classical gravitational problem. Our conclusions thus hold above the critical speed $U*$, which in our case ($\rho_s/\rho \approx 1.2$, $R \approx 4\,\mathrm{mm}$) is approximately $10\,\mathrm{cm\,s^{-1}}$, much smaller than the impact speeds ($\approx 10\,\mathrm{m\,s^{-1}}$).

3.2. Lift

Along the direction $\underline{n}$, the equation of motion can be written as

$$M\left(1 + C_\mathrm{M}\frac{\rho}{\rho_s}\right) U^2\frac{\mathrm{d}\theta}{\mathrm{d}s} = F_\mathrm{L}, \tag{4}$$

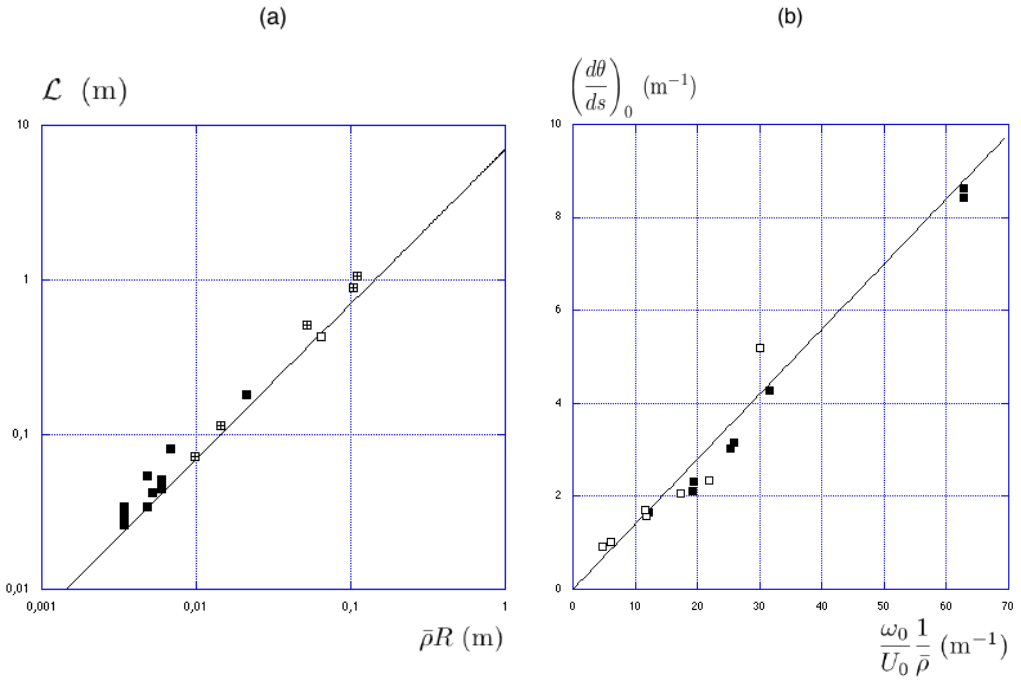

Figure 5. (a) Characteristic length of penetration $\mathcal{L}$ as a function of $\bar{\rho}R$. The symbols ⊞ and □ show the results of May [19] and Truscott and Techet [31], respectively. The symbol ■ is used for our results. Equation (3), that is $\mathcal{L} \approx 7\bar{\rho}R$, is represented by the solid line. (b) Initial curvature $(\mathrm{d}\theta/\mathrm{d}s)_0$ of the ball trajectory as a function of $\omega_0/U_0 \cdot 1/\bar{\rho}$. The symbol □ is used for the data of Truscott and Techet [31] and the symbol ■ for our results. The solid line shows the fit of $(\mathrm{d}\theta/\mathrm{d}s)_0 = 0.14\omega_0/U_0 \cdot 1/\bar{\rho}$.

where $F_\mathrm{L} = \rho\Gamma U RC_n$ is the lift force resulting from the circulation $\Gamma = 2\pi R^2\omega$. In the limit of low Reynolds numbers ($Re < 1$), Rubinow and Keller [26] have shown that we have $C_n = 1/2$. For large Reynolds numbers ($Re \approx 10^5$), Nathan [21] collected the data obtained by several authors on the lift force experienced by spinning balls in air. From these results, we deduce $C_n \approx 0.13$.

Since our experiments are done in water with an entrained air cavity, we found it useful to measure C_n. For this purpose, we focused on the impact region ($s < \mathcal{L}$), where the dynamical parameters (U, ω) are constant, so that equation (4) predicts a constant curvature for the ball trajectory,

$$\left(\frac{\mathrm{d}\theta}{\mathrm{d}s}\right)_0 = \frac{3}{2}\frac{C_n}{\bar{\rho}}\frac{\omega_0}{U_0}. \tag{5}$$

This initial curvature is presented in figure 5(b) as a function of the inverse length $\omega_0/\bar{\rho}U_0$ (■). In the same figure, we also report the data extracted from Truscott and Techet [31] (□). Equation (5) nicely predicts the initial curvature of the trajectory, and the best fit on both sets of data suggests $C_n \approx 0.1$, a value comparable to the one deduced from Nathan [21]. There again, the air cavity behind the ball does not affect the evaluation of the lift, a consequence of the entrainment of a water boundary layer around the projectile.

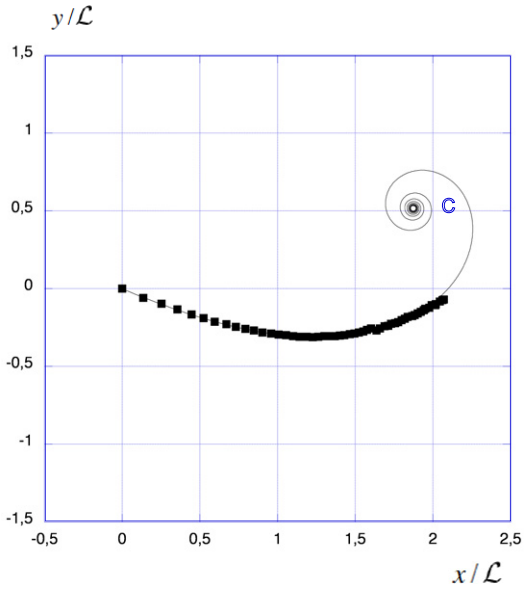

Figure 6. Characteristics of the ideal spiral for a spinning ball: the trajectory of the ball is plotted in the plane (x, y) for $U_0 = 32\,\mathrm{m\,s^{-1}}$, $R = 3.6\,\mathrm{mm}$, $\theta_0 = 67°$, $\omega_0 = 743\,\mathrm{rad\,s^{-1}}$ and $\rho_s/\rho = 1.4$. The experimental data are presented with the ■ symbol, while the theoretical shape (equation (6)) is drawn with a solid thin line ($y = 0$ is the surface of the water bath).

3.3. The ideal spiral

The next step in the derivation of the ball trajectory is to assume that the circulation Γ remains (almost) constant during the motion, that is, over timescale τ. This assumption is suggested by figure 4(c) and we discuss it further in section 3.4. Then, for $\Gamma = 2\pi R^2\omega_0$, equation (4) together with (2) implies

$$\theta(s) = \theta_0 + \Delta S\,\left[\mathrm{e}^{s/\mathcal{L}} - 1\right], \tag{6}$$

where $\Delta = 4C_n/C_\mathrm{D} \approx 1$ and $S = \omega_0 R/U_0$. The deviation of the ball from its initial orientation θ_0 thus increases exponentially with the curvilinear coordinate s, which defines the spinning ball (ideal) spiral. The characteristic length $\mathcal{L}$ for which the spiral coils up precisely is the penetration length expressed by equation (3).

We compare in figure 6 the observed trajectory (■) to equation (6) (solid line). The comparison is made in the plane (x, y) using the geometrical relations $\mathrm{d}x/\mathrm{d}s = \sin\theta$, $\mathrm{d}y/\mathrm{d}s = -\cos\theta$ and for $S \approx 0.09$, the value of the spin parameter in this experiment. The theoretical prediction is in close agreement with the experimental path up to the point where the ball escapes from the bath, whose surface is defined by $y = 0$.

An ideal spiral would converge to a centre C (figure 6) located at a distance D from the impact point. Since C is approached when $\theta(s) - \theta_0$ is of the order of π (corresponding to a U-turn of the ball), we obtain from equation (6) $D \approx \mathcal{L}\ln[1 + \pi/\Delta S]$. The distance D is a linear function of $\mathcal{L}$ and slowly diverges (as $\ln 1/S$) when the spin number goes to 0. Conversely, for large spin numbers, the spiral centre is expected to converge towards the impact location ($D \approx \mathcal{L}/S$).

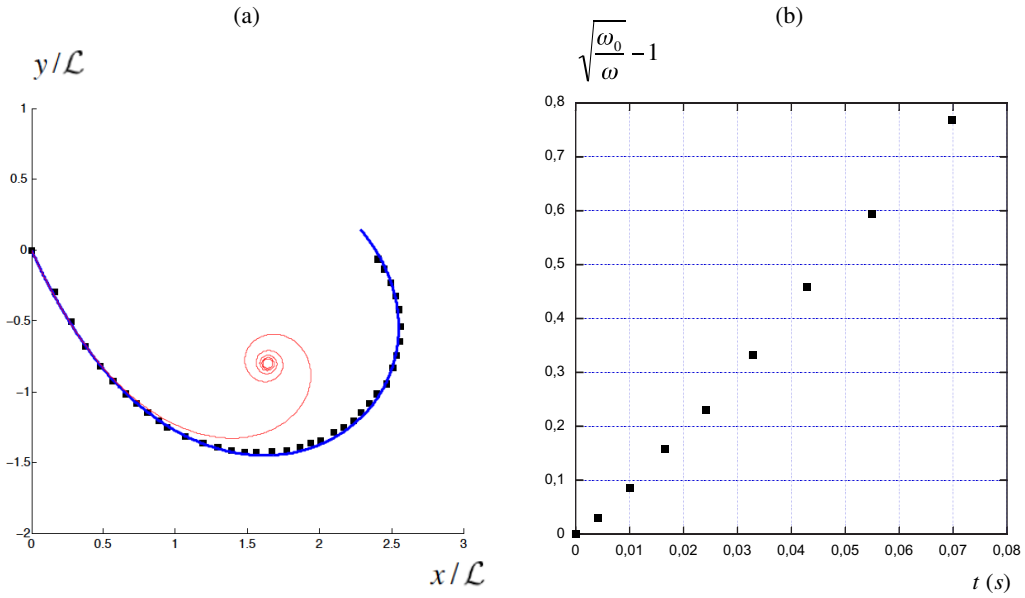

Figure 7. Spinning ball spiral obtained with $R = 3.5\,\text{mm}$, $\rho_s/\rho = 1$, $U_0 = 31\,\text{m}\,\text{s}^{-1}$, $\omega_0 = 1200\,\text{rad}\,\text{s}^{-1}$ and $\theta_0 = 26°$. (a) Trajectory of the ball in the (x, y) plane (■), compared to both the ideal spiral (thin solid line) and the 'real' spiral (thick solid line). (b) Time evolution of the rotation rate $\sqrt{\omega_0/\omega} - 1$.

3.4. Variation in the rotation speed

The 'ideal' spiral derived in equation (6) is a good approximation for the ball trajectory as long as the rotation speed ω remains close to its initial value ω_0. This assumption is valid for the 'shallow' spiral presented in figures 4 and 6, but cannot be used for the 'deep' spiral displayed in figures 1, 2 and 7. In the latter figure, we first show the ball trajectory (figure 7(a)) and observe that the 'ideal' spiral (thin solid line) only captures the data (■) in the first part of the trajectory ($s < \mathcal{L}$). At larger distances, figure 7(b) makes it clear that the rotation rate of the ball decreases, from ω_0 to $0.3\,\omega_0$ at the end of the movement. This decrease of the rotation speed obviously lowers the lift, so that we expect the actual trajectory to be less curved, as observed in figure 7(a).

In order to model the decrease in ω, we assume that the angular momentum $MR^2\omega$ changes due to the torque of viscous forces acting on the surface of the ball, and we introduced $\nu = \eta/\rho$ for the kinematic viscosity. The viscous torque does not exist without rotation (see figure 3(a)) and originates from the difference in velocity $R\omega$ between the two sides of the ball. The boundary layer thickness associated with the rotation scales as $\sqrt{\nu/\omega}$ (typically of the order of $30\,\mu$m), from which we deduce a viscous stress $\eta R\omega/\sqrt{\nu/\omega}$. Since the stress is applied over the surface area R^2, we obtain the following angular momentum equation, ignoring the numerical coefficients,

$$MR^2\frac{\mathrm{d}\omega}{\mathrm{d}t} \sim -\eta\frac{R\omega}{\sqrt{\nu/\omega}}R^3. \tag{7}$$

Equation (7) can be integrated, which leads to the time evolution of ω,

$$\frac{\omega}{\omega_0} = \frac{1}{(1+t/\tau_\omega)^2}, \quad \text{where } \tau_\omega = \frac{1}{\beta}\frac{\rho_s}{\rho}\frac{R}{\sqrt{\omega_0 \nu}}. \tag{8}$$

The spin velocity of the ball thus decreases over a characteristic time τ_ω (where β is a numerical constant, whose value is discussed below). The trajectory remains close to the ideal spiral as long as the travelling time $t(s) = \tau(e^{s/\mathcal{L}} - 1)$ is smaller than τ_ω (we recall that $\tau = \mathcal{L}/U_0$). One thus expects to leave the ideal spiral when s becomes larger than $\mathcal{L}\ \ln[1 + U_0/\sqrt{\omega_0 \nu}\,]$, that is, a few times $\mathcal{L}$, as observed in figure 7.

Conversely, if $\tau_\omega < \tau$, ω decreases quicker than needed to make the spiral, and the corresponding lift force vanishes before curving the trajectory. One thus expects a linear propagation of the ball in this limit, which corresponds to impacts in viscous liquids ($\nu > U_0^2/\omega_0$). For the parameters in our experiments ($U_0 \approx 30\,\mathrm{m\,s^{-1}}$; $\omega_0 \approx 1000\,\mathrm{rad\,s^{-1}}$), this limit corresponds to oils at least 1000 times more viscous than water.

3.5. The 'real' spiral

In order to account for the variation in the spin rate during the ball motion, we re-write the equation of motion along the $\underline{n}$-direction (4) as an equation for the curvature,

$$\frac{\mathrm{d}\theta}{\mathrm{d}s} = \frac{\Delta S}{\mathcal{L}} e^{s/\mathcal{L}} \frac{\omega}{\omega_0}. \tag{9}$$

Since $\omega/\omega_0 = 1/(1 + \tau/\tau_\omega(e^{s/\mathcal{L}} - 1))^2$, this equation can be integrated, which yields

$$\theta(s) = \theta_0 + \Delta S \frac{e^{s/\mathcal{L}} - 1}{\left[1 + \frac{\tau}{\tau_\omega}(e^{s/\mathcal{L}} - 1)\right]}. \tag{10}$$

In the limit $\tau/\tau_\omega \ll 1$, the evolution of the local angle reduces to the ideal spiral (6). However, even if τ/τ_ω is small, its product with the exponential term $e^{s/\mathcal{L}}$ can lead to an observable effect of the spin decrease. For $\beta = 3.1$, the trajectory obtained with equation (10) is drawn with a thick solid line in figure 7(a), showing fair agreement with the data. At long distances, equation (10) predicts that the ball follows a straight line, deviating from the impact direction by an angle $\Delta S \tau_\omega/\tau$ proportional to the spin number S.

4. Application to sports

The physical origin of the spinning ball spiral lies in the difference in velocity dependences of lift and drag, which are linear and quadratic, respectively. This behaviour is specific to high Reynolds number flows around spinning spheres. In our experiments, we used water to minimize the effect of gravity and to reduce the spatial scale of the spiral $\mathcal{L} \sim \bar{\rho} R$. However, the spinning ball spiral should also exist in air, and we discuss here its influence in ball games.

For different sports, table 1 shows the ball size, the density ratio, the maximum ball velocity, the characteristic spin parameter and the size of the field, L. In the special case of baseball, L represents the distance between the pitcher and the batter. Using these data, we also display the penetration length $\mathcal{L} = 7\bar{\rho}R$ and the length scale U_0^2/g on which gravity acts. By comparing $\mathcal{L}$ and U_0^2/g, one can identify sports dominated by aerodynamics (table tennis, golf and tennis) and sports dominated by gravity (basketball and handball). In between, we

Table 1. Specifications for different sports. The first three sports are dominated by aerodynamic effects ($\mathcal{L} \ll U_0^2/g$). For the last two sports, gravity dominates aerodynamics ($\mathcal{L} \gg U_0^2/g$). In between, we identify sports for which both gravity and aerodynamics can be used to control the ball's trajectory. In this table, L is the size of the field except for baseball, where it stands for the distance between the pitcher and the batter.

Sport	$2R$ (cm)	ρ_s/ρ	U_0 (m s^{-1})	$S = R\omega_0/U_0$	L (m)	$\mathcal{L}$ (m)	U_0^2/g (m)	d (m)
Table tennis	4.0	67	50	0.36	2.7	9.3	255	1
Golf	4.2	967	90	0.09	200	141	826	7
Tennis	6.5	330	70	0.19	24	73	499	5
Soccer	21	74	30	0.21	100	54	92	7
Baseball	7.0	654	40	0.17	18	160	163	7
Volleyball	21	49	20	0.21	18	35	41	5
Basketball	24	72	10		28	60	10	
Handball	19	108	20		40	71	40	

find sports where both gravity and aerodynamics play a comparable role (soccer, volleyball and baseball). Indeed, in the first category of sports, the spin is systematically used, while it is not relevant in the second category, and it only appears occasionally in the third one, in order to produce surprising trajectories.

Focusing on sports where aerodynamics plays a role, we observe that the penetration length, which is also the characteristic length of the spiral, is generally larger than the size of the field. Since the spin parameter is smaller than one, the spiral centre (section 3.3) will lie outside the field. This suggests that the ball trajectory (6) can be expanded for $s/\mathcal{L} \ll 1$. In this limit, the spiral reduces to a circle of curvature (5), and we can evaluate the length d by which the ball deviated from its initial direction by its own size R: $d \approx \sqrt{2\mathcal{L}R/\Delta S}$. This distance is shown in the last column of table 1. It is found to be systematically smaller than L, the field size, which makes relevant the use of spin effects to control the trajectory of the ball.

The case of soccer, where $\mathcal{L}$ is twice as small as L, is worth commenting on. The ball trajectory can deviate significantly from a circle, provided that the shot is long enough. Then the trajectory becomes surprising and somehow unpredictable for a goalkeeper. This is the way we interpret a famous goal by the Brazilian player Roberto Carlos against France in 1997 (http:// www.youtube.com/watch?v=crSkWaJqx-Y). This free kick was shot from a distance of approximately 35 m, that is, comparable to the distance $\mathcal{L}$ for which we expect this kind of unexpected trajectory. Provided that the shot is powerful enough, another characteristic of Roberto Carlos' abilities, the ball trajectory brutally bends towards the net, at a velocity still large enough to surprise the keeper.

5. Conclusions

We have studied the motion of spinning spheres at high Reynolds number and in the limit of low gravity. In this regime, we showed that the curvature of the ball trajectory changes as it moves,

following law (9), rewritten here as

$$\frac{\mathrm{d}\theta}{\mathrm{d}s} \sim \frac{\omega(s)}{U(s)} \cdot \frac{1}{\bar{\rho}}. \tag{11}$$

We have identified the characteristic length $\mathcal{L} \sim 7\bar{\rho}R$ over which the ball slows down and coils. Using this length, we have classified different phases in the ball trajectory. (i) In the initial phase ($s/\mathcal{L} \ll 1$), neither the velocity nor the spin varies, and the ball follows a circular path whose curvature C_0 can be deduced from (11): $\omega_0/\bar{\rho}U_0$. (ii) As s approaches $\mathcal{L}$, the velocity is changed but the spin is only weakly affected. This difference in behaviour is all the larger since dimensionless number $\sqrt{\omega_0 \nu}/U_0$ is small. In this phase ($s/\mathcal{L} \approx 1$), the spinning ball coils up and forms a spiral. (iii) The last phase of the flight is reached when both the velocity and the spin decrease ($s/\mathcal{L} > 1$). The trajectory then deviates from the spiral and tends to a straight line as the ball stops.

References

[1] Achenbach E 1972 Experiments on the flow past spheres at very high Reynolds numbers *J. Fluid Mech.* **54** 565–75

[2] Barkla H M and Auchterloniet L J 1971 The Magnus or Robins effect on rotating spheres *J. Fluid Mech.* **47** 437–47

[3] Batchelor G K 1967 *An Introduction to Fluid Dynamics* (Cambridge: Cambridge University Press)

[4] Benjamin T B 1993 Note on formulas for the drag of a sphere *J. Fluid Mech.* **246** 335–42

[5] Bergmann R P H M, van der Meer D, Gekle S, van der Bos J A and Lohse D 2009 Controlled impact of a disk on a water surface: cavity dynamics *J. Fluid Mech.* **633** 381–409

[6] Coriolis G 1835 *Théorie Mathématique des Effets du Jeu de Billard* (Paris: Jacques Gabay Editeur) http://gallica.bnf.fr/ark:/12148/bpt6k29318f.image.f1

[7] Cross R 1998 The trajectory of a ball in lawn bowls *Am. J. Phys.* **66** 735–8

[8] Davies C N 1945 *Proc. Phys. Soc.* **57** 259

[9] Davies J M 1949 The aerodynamics of golf balls *J. Appl. Phys.* **20** 821–8

[10] Duclaux V, Caille F, Duez C, Ybert C, Bocquet L and Clanet C 2007 Dynamics of transient cavities *J. Fluid Mech.* **591** 1–19

[11] Duez C, Ybert C, Clanet C and Bocquet L 2007 Making a splash with water repellency *Nature Phys.* **3** 180–3

[12] Eiffel G 1909 *Recherches expérimentales sur la résistance de l'air exécutées à la tour Eiffel* (Paris: Librarie aéronautique) http://gallica.bnf.fr/ark:/12148/bpt6k5675046x.zoom.r=Eiffel.f11.langFR

[13] Galilei G 1638 *Dialogues Concerning Two New Sciences* (New York: Dover) http://gallica.bnf.fr/ark:/12148/bpt6k512641.image.f2.langFR

[14] Geiger H and Marsden E 1909 On a diffuse reflection of the α-particles *Proc. R. Soc.* A **82** 495–500

[15] Glasheen J W and McMahon T A 1996 A hydrodynamic model of locomotion in the basilisk lizard *Nature* **380** 340–2

[16] Lohse D 2003 Bubble puzzles *Phys. Today* **56** 36–41

[17] Lyotard N, Shew W L, Bocquet L and Pinton J-F 2007 Polymer and surface roughness effects on the drag crisis for falling spheres *Eur. Phys. J.* B **60** 469–76

[18] Magnus G 1853 Über die Abweichung der Geschosse, und: Über eine abfallende Erscheinung bei rotirenden Körpern *Annalen der Physik* **164**(1) 1–29

[19] May A 1950 The virtual mass of a sphere entering water vertically *J. Appl. Phys.* **21** 1285–9

[20] Metha D 1985 Aerodynamics of sports balls *Annu. Rev. Fluid Mech.* **17** 151–89

[21] Nathan A M 2008 The effect of spin on the flight of a baseball *Am. J. Phys.* **76** 119–24

[22] Newton I 1687 *Philosophiæ Naturalis Principia Mathematica* **lib. 2** prop. 33

[23] Oseen C W 1910 Über die Stokes'sche Formel, und über eine verwandte Aufgabe in der Hydrodynamik *Ark. Math. Astronom. Fys.* **6** No. 27
[24] Pruppacher H R 1968 An experimental determination of the drag on a sphere at low Reynolds numbers *J. Appl. Phys.* **39** 4129–32
[25] Robins B 1805 *New Principles of Gunnery* ed R Hutton (first printed in 1742)
[26] Rubinow S I and Keller J B 1961 The transverse force on a spinning sphere moving in a viscous fluid *J. Fluid Mech.* **11** 447–59
[27] Rutherford E 1906 *Phil. Mag. Ser. 6* **12** 143
[28] Schlichting H 1955 *Boundary-Layer Theory* (New York: McGraw-Hill)
[29] Smith M R, Hilton D K and Van Sciver S W 1999 Observed drag crisis on a sphere in flowing He I and He II *Phys. Fluids* **11** 751–3
[30] Stokes G G 1851 On the effect of internal friction of fluids on the motion of pendulums *Trans. Camb. Phil. Soc.* **9** 8–106
[31] Truscott T T and Techet A H 2009 Water entry of spinning spheres *J. Fluid Mech.* **625** 135–65
[32] Worthington A M and Cole R S 1900 Impact with a liquid surface studied by the aid of instantaneous photography. Paper II *Phil. Trans. R. Soc.* A **194** 175–99